Physica Medica 64 (2019) 74–80

Contents lists available at ScienceDirect

Physica Medica

journal homepage: www.elsevier.com/locate/ejmp

Technical note

Response of a nanoDot OSLD system in megavoltage photon beams

Kento Hoshida[a], Fujio Araki[b,*], Takeshi Ohno[b], Ikuo Kobayashi[c]

[a] Graduate School of Health Sciences, Kumamoto University, 4-24-1 Kuhonji, Kumamoto 862-0976, Japan
[b] Department of Health Sciences, Faculty of Life Sciences, Kumamoto University, 4-24-1 Kuhonji, Kumamoto 862-0976, Japan
[c] Nagase Landauer Ltd., Block C22-1, Suwa, Tsukuba, Ibaraki 300-2686, Japan

ARTICLE INFO

Keywords:
nanoDot optically stimulated luminescence dosimeter (OSLD)
Megavoltage photon beams
Energy response
Monte Carlo simulation

ABSTRACT

Purpose: The aim of this study was to investigate the response of a nanoDot optically stimulated luminescence dosimeter (OSLD) system in megavoltage photon beams.
Methods: The nanoDot response was compared with the ionization chamber measurements for 4–18-MV photons in a plastic water phantom. The response was also calculated by the Monte Carlo method. In addition, the perturbation correction factor, P_Q, in the nanoDot cavity was calculated according to the Burlin's cavity theory. The angular dependence of the nanoDot was evaluated using a spherical phantom.
Results: The calculated and measured nanoDot responses at a 10-cm depth and 10 × 10-cm^2 field were in agreement within 1% for 4–18-MV. The response increased by 3% at a 20 × 20-cm^2 field for the lower energy of 4 MV; however, it was constant within ± 1% for 6–18 MV. The response was in a range from 1.0 to 0.99 for mean photon energy of more than 1.0 MeV but it increased with less than the 1.0 MeV. P_Q for the nanoDot cavity was approximately constant at 0.96–0.97 for greater than and equal to 10 MV. The angular dependence decreased by 5% and 3% for 6 and 15 MV, respectively.
Conclusions: The nanoDot was energy-independent in megavoltage photon beams.

1. Introduction

Recently, an optically stimulated luminescent dosimeter (OSLD) has become increasingly popular in medical dosimetry for a variety of tasks such as machine output verification [1–3] and in vivo measurements [4]. The nanoDot OSLD system (Landauer, Inc., Glenwood, IL) has numerous advantages over other dosimeters. For example, the nanoDot OSLD system can provide high spatial resolution owing to its small size and minimal fading effect. The OSLD accumulates radiation energy using the same method as a thermoluminescent dosimeter (TLD). However, the readout of the OSLD system uses light instead of heat for a TLD. Thus, its workflow is simpler and faster than that of TLD, and it can provide multiple readings with minimal signal loss. TLDs have recently been replaced with OSLDs in the postal dosimetry audit of megavoltage radiotherapy photon beams at the Imaging and Radiation Oncology Core (IROC) [3] and the Australian Clinical Dosimetry Service (ACDS) [1,2], and with radiophotoluminescent glass dosimeter (RGD) at the International Atomic Energy Agency (IAEA) [5]. Recently, the American Association of Physics in Medicine (AAPM) Task Group (TG)-191 has made recommendations on the clinical use of TLDs and OSLDs. Therefore, the OSLD has attracted attention.

The material of the OSLD device commonly consists of aluminum oxide doped with carbon (Al_2O_3:C). The underlying process of optically stimulated luminescence is similar to thermoluminescence, except for the stimulating process. The free electrons liberated by ionizing radiation are trapped in energy traps within the forbidden energy gap in the energy level of carbon, and this is the dose information. The number of trapped charges is proportional to the amount of radiation the OSLD was exposed to while the subsequent luminescence depends on not just the radiation dose of exposure but the duration, intensity and wavelength of the optical stimulation. The MicroSTARii from Landauer used in this study is the second-generation optical system used to "read-out" nanoDot dosimeters and has been shown to be highly reproducible in its optical stimulation readout procedure [6].

Some studies [7–12] have demonstrated the energy dependence of OSLD at megavoltage photon beams and have reported that the energy dependence was negligible or small. The angular dependence, which could be a disadvantage owing to the shape of the nanoDot detector, has also been investigated in some studies [12–15]. Kim et al. [12] concluded that there was no angle dependency with a cylindrical phantom for nanoDot OSLD. Conversely, Kerns et al. [13] and Lehmann et al. [14] reported a 4% and 2% angular dependence for the nanoDot, respectively, using rectangular phantoms. Jursinic et al. [15] reported a maximum angular dependence of 1% or less for nanoDot dosimetry in

* Corresponding author at: Department of Health Sciences, Faculty of Life Sciences, Kumamoto University, 4-24-1 Kuhonji, Chuo-ku, Kumamoto 862-0976, Japan.
E-mail address: f_araki@kumamoto-u.ac.jp (F. Araki).

https://doi.org/10.1016/j.ejmp.2019.06.014
Received 19 February 2019; Received in revised form 16 June 2019; Accepted 25 June 2019
Available online 28 June 2019
1120-1797/ © 2019 Associazione Italiana di Fisica Medica. Published by Elsevier Ltd. All rights reserved.

Table 1
Dosimetric parameters and nanoDot response calculated from the MC simulation and Burlin's cavity theory for 4–18-MV photon beams. The response is calculated at a depth of 10 cm for a 10 × 10-cm^2 field in solid water.

Energy MV	$TPR_{20,10}$	1-*d*	$\left(\frac{\bar{\mu}_{en}}{\rho}\right)^{SW}_{nanoDot}$	$\left(\frac{\bar{L}}{\rho}\right)^{SW}_{nanoDot}$	$\left(\frac{D_{SW}}{D_{nanoDot}}\right)_{MC}$	$(f^{SW}_{nanoDot})_{Burlin}$	P_Q	$(F^Q_{6MV})_{MC}$	$(F^Q_{6MV})_{Burlin}$
4	0.617	0.189	1.080	1.223	1.131	1.196	0.946	1.012	1.002
6	0.663	0.119	1.079	1.215	1.144	1.199	0.954	1.000	1.000
10	0.739	0.065	1.052	1.204	1.148	1.194	0.962	0.996	1.004
15	0.757	0.049	1.034	1.200	1.151	1.192	0.965	0.994	1.006
18	0.779	0.038	1.009	1.195	1.150	1.188	0.967	0.995	1.009

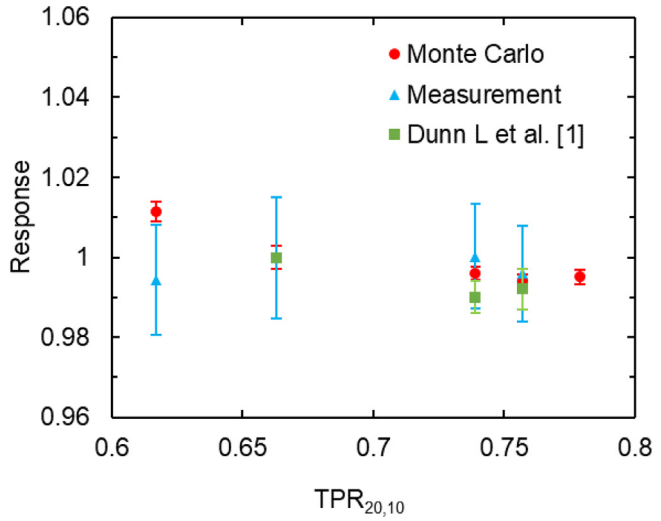

Fig. 1. MC-calculated and measured nanoDot response as a function of $TPR_{20,10}$ at the reference condition (depth: 10 cm, field size: 10 × 10 cm^2). The response is normalized at 6 MV ($TPR_{20,10}$ = 0.663).

various phantoms. In addition, Viatcheslav et al. [16] developed a comprehensive end-to-end test for head and neck intensity modulated radiation therapy (IMRT) treatments by the nanoDot dose measurement. Brian et al. [17] carried out an end-to-end test in some clinics, and the consistency of their results indicated that the nanoDot system could be used for high-precision radiotherapy. The nanoDot is expected to be a quality assurance (QA) tool for high-precision radiotherapy in the future.

In this study, the beam energy response of the nanoDot was investigated at the reference conditions for 4–18 MV photon beams, from experimental measurements and Monte Carlo (MC) simulations. The factors responsible for the response in the photon beams were analyzed as a function of the energy, field size, and depth from the MC simulations, according to the Burlin general cavity theory. The angular dependence was also investigated using a spherical phantom.

2. Materials and methods

2.1. nanoDot OSLD system

The OSLD used in this study was InLight nanoDot (Landauar, Inc., Glenwood, IL). The sensitive material is a disk with a 5-mm diameter and a 0.2-mm thickness and consisted of aluminum oxide doped with carbon (Al_2O_3:C). The disk is encased in a 1.0 × 1.0 × 0.2 cm^3 light-tight plastic case and is sandwiched between thin polyester films. The effective atomic number and density of the disk are 11.28 and 1.41 g/cm^3, respectively [10,15]. The readout of the nanoDot was obtained by an InLight microSTARii reader (Landauar, Inc., Glenwood, IL). The microSTARii was recently developed, and it is specialized for medical dosimetry. The signal-to-noise ratio has been improved compared to that of a conventional microSTAR; therefore, the readout is accurate, stable, and repeatable with minimal signal loss [6].

2.2. Experimental measurements

2.2.1. Signal uniformity and reproducibility

First, the nanoDot system was calibrated by comparing the absolute dose measured with a PTW 30013 ionization chamber at a 10-cm depth for a 20 × 20-cm^2 field with a source-axis-distance (SAD) of 100 cm, and the ionization chamber was calibrated with the absorbed dose-to-water for ^{60}Co, according to the International Atomic Energy Agency (IAEA) dosimetry protocol [18]. The signal uniformity and reproducibility of the sixty nanoDots used in this study were also evaluated. To determine the individual calibration coefficient, N_i (mGy/count), 1.0 Gy with 6 MV was delivered to each nanoDot in a solid water phantom [at 10-cm depth for a 20 × 20-cm^2 field with SAD of 100 cm] and the measurements were then repeated three times. The nanoDots were positioned in a solid water phantom RMI-457 (GAMMEX RMI, Wisconsin) with the dimensions of 30 × 30 × 20 cm^3 and were irradiated with a beam direction perpendicular to the nanoDot. The *Ni* for the sixty nanoDots was obtained from the average of five readouts.

2.2.2. Energy dependence

The energy response of the nanoDot was investigated by comparing the ionization chamber measurements. The irradiation condition was set to the reference conditions with a depth of 10 cm for a 10 × 10-cm^2 field and an SAD of 100 cm in a solid water phantom. Each nanoDot was irradiated by 100 monitor units (MUs) with dose rates of 600 MU/min. Six nanoDots were used for the measurements of each photon energy response. The irradiation for each nanoDot was performed by individually inserting the nanoDot into the phantom. The absorbed dose (mGy) of each nanoDot was given by the following equation.

$$D_i = \bar{M}_{raw,i} \cdot N_i \cdot k_L. \quad (1)$$

The parameter $\bar{M}_{raw,i}$ is the average count of five readouts. The k_L is a dose non-linearity correction factor and it was set to 1.0 in this study because the nanoDot response has the dose linearity up to 2.0 Gy according to previous studies [2,8,11]. The fading correction is included in *Ni* because every readout is in the same time period after irradiation as the dose calibration. The absorbed dose was also measured using a PTW 30013 Farmer-type ionization chamber (cavity volume of 0.6 cm^3 with length of 23.0 mm and radius of 3.05 mm, PTW-Freiburg, Germany) using the same conditions.

The photon energies used in the measurements were 4 MV ($TPR_{20,10}$ = 0.637) and 10 MV ($TPR_{20,10}$ = 0.733) from an Elekta Synergy linear accelerator (Elekta, Stockholm, Sweden) and 6 MV ($TPR_{20,10}$ = 0.663) and 15 MV ($TPR_{20,10}$ = 0.757) from a Varian Clinac iX linear accelerator (Varian Oncology Systems, Palo Alto, CA). The beam quality index $TPR_{20,10}$ is defined as the tissue phantom ratio in water at depths of 20 and 10 cm for a 10 × 10-cm^2 field and a source-chamber distance of 100 cm [18].

2.2.3. Angular dependence

The individual nanoDots were inserted into a Gamma Knife spherical phantom with a radius of 8 cm. The angular dependence was

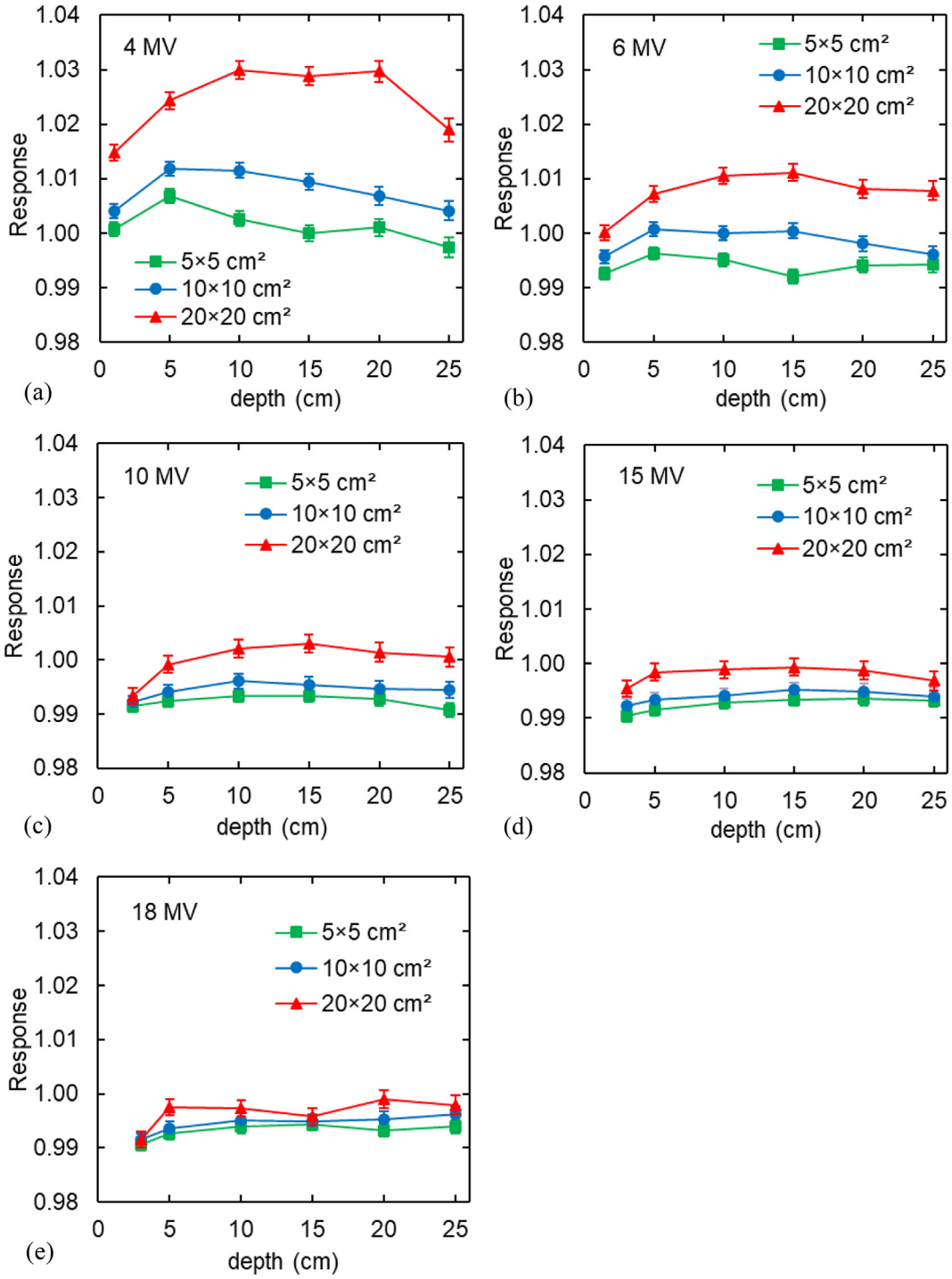

Fig. 2. MC-calculated nanoDot response as a function of the depth and field size for 4–18-MV photon beams. The response is obtained from the ratio of $D_{SW}/\bar{D}_{nanoDot}$ and is normalized at a depth of 10 cm for a 10 × 10-cm^2 field for a 6-MV photon beam.

measured at a 5 × 5-cm^2 field for the photon energies of 6 MV and 15 MV from a Varian Clinac iX linear accelerator. The nanoDots were measured by gantry angles from 0 to 90 degrees and from 270 to 330 degrees and were reversed for the irradiation angles of 120–240 degrees to avoid the influence of the couch and support frame. The measurements were performed every 30 degrees, and three nanoDots were used at each angle. The absorbed dose for the gantry angles was also measured by a PTW 31010 ionization chamber, and the angular response was within 1% for the spherical phantom.

2.3. Monte Carlo simulations

2.3.1. nanoDot OSLD modeling

The nanoDot has been modeled in previous studies [12,14] using the Electron Gamma Shower at National Research Council of Canada (EGSnrc) c++ based egs_chamber user code [19,20]. The nanoDot detector is composed of 73.1% Al_2O_3 and 26.9% polyester; however, the scored dose is only from the deposition in Al_2O_3. In this study, the nanoDot dose was scored as 100% Al_2O_3 (ρ = 1.41 g/cm^3).

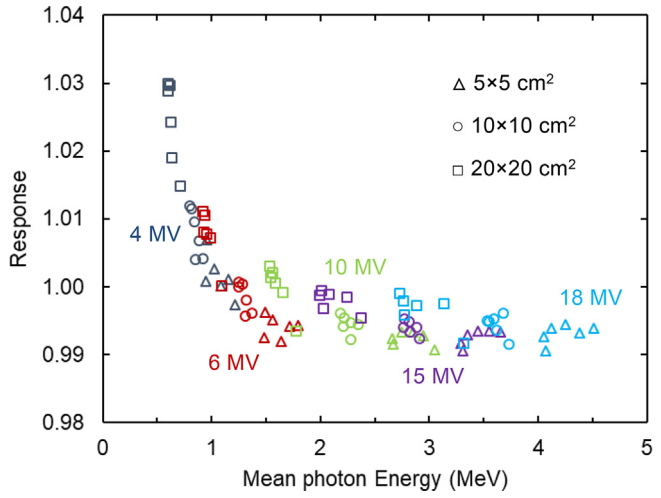

Fig. 3. MC-calculated nanoDot response as a function of mean photon energy. The response is calculated from Eq. (1) and it is normalized at a depth of 10 cm for a 10 × 10 cm^2 field for a 6 MV photon beam.

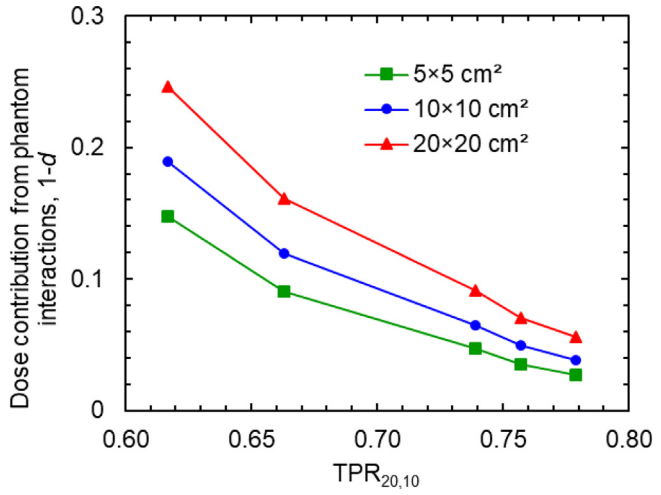

Fig. 4. Dose contribution from the photon interactions (1-*d*) in the nanoDot cavity as a function of $TPR_{20,10}$ at a depth of 10 cm for 5 × 5, 10 × 10, and 20 × 20-cm^2 fields. The error bars are smaller than the symbols used in plots.

2.3.2. Energy dependence and field size and depth dependence

The irradiation conditions for the MC simulations were set to the field sizes of 5 × 5, 10 × 10, and 20 × 20 cm^2 at depths of d_{max} (depth of maximum dose), 5, 10, 15, 20, and 25 cm with an SAD of 100 cm for the energies of 4-, 6-, 10-, 15-, and 18-MV photon beams. The photon spectra were derived from the phase space data from a Varian linear accelerator for 6, 15, and 18 MV and an Elekta linear accelerator for 4 and 10 MV, using the EGSnrc/BEAMnrc code [21,22]. The photon energies used in the simulations are listed in Table 1. The accuracy of the beam modeling for the MC simulations was verified by comparing the corresponding measured percent depth dose and cross-beam profiles for the field sizes in water listed above. The nanoDot response was analyzed from the ratio between the absorbed doses to solid water and the nanotDot disk (Al_2O_3).

2.3.3. Burlin's general cavity theory for the nanoDot cavity material

The factor responsible for the photon energy dependence and field size and depth dependence of the nanoDot was analyzed according to the Burlin's general cavity theory [23]. Burlin proposed the cavity theory for photons for all cavity sizes, which approaches the Spencer-Attix theory [24] in the small size limit and the ratio of the mass energy-absorption coefficient for large cavities. In this study, the Burlin's cavity theory was given by

$$D_{med} = \bar{D}_{cav} f_{cav}^{med} P_Q, \tag{2}$$

$$f_{cav}^{med} = d(\bar{L}/\rho)_{cav}^{med} + (1-d)(\bar{\mu}_{en}/\rho)_{cav}^{med}. \tag{3}$$

Hence, P_Q can be obtained as follows:

$$P_Q = (D_{med}/\bar{D}_{cav})/f_{cav}^{med}, \tag{4}$$

where D_{med} is the dose that would have been delivered to the medium in the absence of the cavity. The parameter $\bar{D}_{cav}$ is the average dose delivered to the cavity, and f_{cav}^{med} is a factor that varies with the energy, radiation type, medium size, and composition of the cavity. The parameter P_Q is a perturbation correction factor of the nanoDot in the medium, and $(\bar{L}/\rho)_{cav}^{med}$ is the average restricted mass collision stopping-power ratio of the medium to the cavity. The parameter $(\bar{\mu}_{en}/\rho)_{cav}^{med}$ is the ratio of the mass energy absorption coefficients, the medium to the cavity, averaged over the photon energy fluence spectrum present in the medium. The parameter *d* represents the attenuation of the electrons across the cavity and can be thought of as the proportion of secondary electrons generated in the medium that is absorbed in the cavity. The parameter (1-*d*) represents the electrons generated in the cavity and can be considered the dose contribution from the electrons generated by the photon interactions in the cavity. Therefore, *d* for the nanoDot cavity can be calculated with the MC simulations as the fraction of the dose component resulting from the photon interactions in the medium to the total dose in the nanoDot. The parameter (1-*d*) can be calculated as the fraction of the dose component resulting from the photons in the nanoDot cavity.

In Eq. (2), the dose to water, D_{SW}, was calculated with the size of a 5-mm radius and 0.2-mm thickness as well as the nanoDot disk. The nanoDot dose, $\bar{D}_{nanoDot}$, was scored in the Al_2O_3 disk, as shown in Fig. 1. The center of the scoring volume for D_{SW} and $\bar{D}_{nanoDot}$ was assumed to be the same depth in solid water. The parameter $(\bar{L}/\rho)_{nanoDot}^{SW}$ of the solid water to the nanoDot was calculated from phase space data using the EGSnrc/SPRRZnrc code [25]. The parameter $(\bar{\mu}_{en}/\rho)_{cav}^{med}$ was calculated by the ratio of collision kerma for solid water to the nanoDot as follows:

$$\left(\frac{\bar{\mu}_{en}}{\rho}\right)_{nanoDot}^{SW} = \frac{\sum_i E_i[\Phi(E_i)(\mu_{en}(E_i)/\rho)]_{SW}\Delta E_i}{\sum_i E_i[\Phi(E_i)(\mu_{en}(E_i)/\rho)]_{nanoDot}\Delta E_i}, \tag{5}$$

where E_i is the photon energy at the midpoint of energy bin *i*. The parameter $\Phi(E_i)$ is the photon fluence in energy bin *i*, and $[\mu_{en}(E_i)/\rho]$ is the mass energy-absorption coefficients for energy E_i. The parameterΔE_i is the width of energy bin *i*, and $\mu_{en}(E_i)/\rho$ for each photon energy is obtained from the data of Seltzer and Hubbell [26]. The photon fluence spectra were calculated from the phase space data at the reference depth for a 10 × 10-cm^2 field using the EGSnrc/FLURZnrc code [25]. The photon and electron cutoff energies for the SPRRZnrc and FLURZnrc codes were set to 0.01 MeV and 0.521 MeV, respectively.

2.3.4. Angular dependence

The angular dependence of the nanoDot was calculated at a 5 × 5-cm^2 field for the photon energies of 6 MV and 15 MV using the EGSnrc c + + based egs_chamber user code. The geometrical setup of the nanoDot was the same as the experimental measurements. The nanoDot was irradiated every 10 degrees from 0 to 360 degrees.

2.3.5. Calculation parameter

In the egs_chamber, photoelectron angular sampling, atomic relaxation, spin-effect, and electron impact ionization were included. The XCOM database [27] from the National Institute of Standards Technology (NIST) was used for the photon cross-sections. Variance reduction techniques were used to further improve the calculation efficiency. The photon cross-section was enhanced from 1 to 128 depending on the geometry and location. The photons were split on the crossing surfaces with a ratio of 1:128, and the Russian Roulette feature was turned on

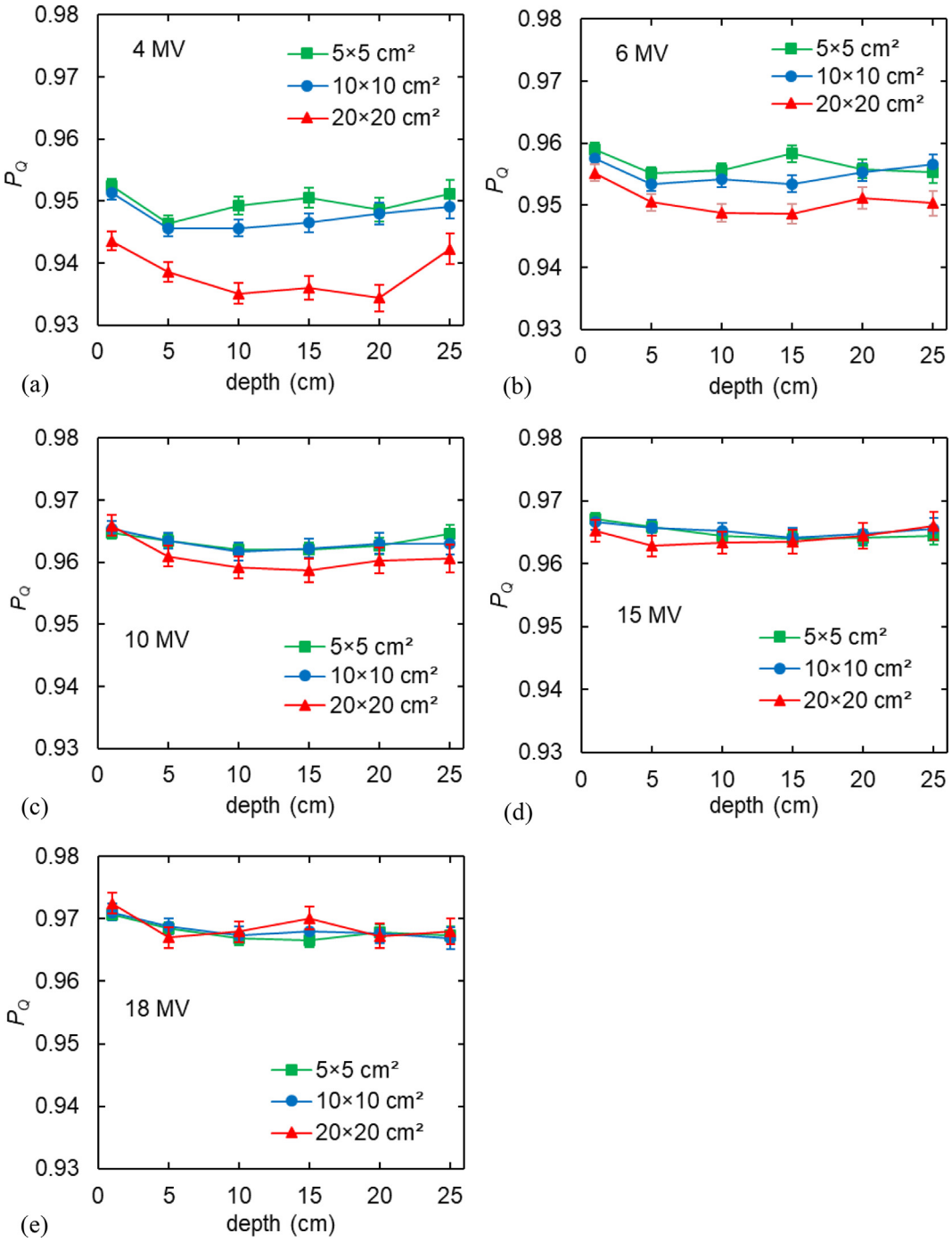

Fig. 5. Perturbation correction factor, P_Q, as a function of the depth and field size for the 4–18-MV photon beams.

for the crossing surfaces with a ratio of 256:1. The cutoff energies of 0.01 MeV and 0.521 MeV were introduced for the photons and electrons, respectively. The parameter (1-*d*) was calculated with the electron cutoff energy of 100 MeV owing to discarding the electrons generated in the surrounding medium and entering the nanoDot disk. The statistical uncertainty (1 standard deviation) of the doses scored in solid water and the nanoDot was less than 0.1%.

3. Results and discussion

3.1. Signal uniformity and reproducibility

The signal uniformity was evaluated by an element correction factor (ECF) as follows:

$$ECF_i = \frac{\bar{M}}{M_i}, \tag{6}$$

where M_i is the raw count of each nanoDot. $\bar{M}$is the average count of sixty nanoDots. The ECF for each nanoDot derived from the dose calibration of three times ranged from 0.90 to 1.09. The average reproducibility of the sixty nanoDots was approximately 3%. This result suggests to use the individual calibration coefficient, *Ni* for each nanDot.

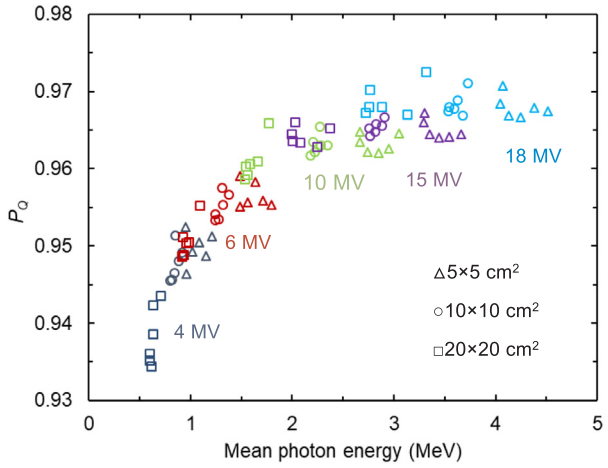

Fig. 6. Perturbation correction factor P_Q of the nanoDot as a function of mean photon energy.

3.2. Energy dependence

The measured and MC calculated nanoDot responses as a function of $TPR_{20,10}$ at a depth of 10 cm for a 10 × 10-cm^2 field are shown in Fig. 1. The nanoDot response was represented as follows:

$$F_6^Q{}_{MV} = \frac{(D_{SW}/\bar{D}_{nanoDot})_{6\ MV}}{(D_{SW}/\bar{D}_{nanoDot})_Q}, \quad (7)$$

where the numerator and denominator are the average dose ratio $D_{SW}/\bar{D}_{nanoDot}$ of solid water to the nanoDot for 6-MV photons and the beam quality Q of interest, respectively. The measured D_{SW} is obtained from the ionization chamber measurements. For the 4–18-MV photons, the measured and MC calculated nanoDot responses were 0.995–1.001 and 1.012–0.994, respectively. The calculated response was in good agreement within 1% with the measured values and previous data [1], except for the 4-MV photons. The calculated nanoDot response was higher for the lower energies of 4 and 6 MV. Viamonte et al. [9] indicated that there was no clear energy dependence of Al_2O_3:C for greater than 6 MV, and the sensitivity was 4% higher for a ^{60}Co beam. In addition, Scarboro et al. [11] reported that the nanoDot energy response was less than 3% different for greater than 1.0 MeV of mean photon energy.

The nanoDot response was also obtained from the Burlin factor $(f_{cav}^{med})_{Burlin}$ given by Eq. (3) as follows.

$$(F_6^Q{}_{MV})_{Burlin} = \frac{(f_{nanoDot}^{SW})_{6\ MV}}{(f_{nanoDot}^{SW})_Q}. \quad (8)$$

The Burlin factor $(f_{nanoDot}^{SW})_{Burlin}$ for each photon energy was calculated from the dosimetric parameters listed in Table 1. The nanoDot response $(F_6^Q{}_{MV})_{Burlin}$ calculated by the Burlin's cavity theory showed approximately a 1% difference to that of the MC calculated response $(F_6^Q{}_{MV})_{MC}$. However, the average dose ratios $D_{SW}/\bar{D}_{nanoDot}$ derived from the MC simulation were 5.8%–3.4% lower than the Burlin estimated $(f_{nanoDot}^{SW})_{Burlin}$ values for 4–18 MV. This is because the fluence of the secondary electrons produced from the photon interactions in the medium is perturbed by the nanoDot cavity. The perturbation correction factor, P_Q, approaches unity as the photon energy increases, as listed in Table 1. The P_Q value was 0.946 for 4 MV and 0.967 for 18 MV.

3.3. Field size and depth dependence

The field size and depth dependence for the nanoDot response were calculated from the MC simulation. The nanoDot response as a function of the field size and depth for 4–18 MV is shown in Fig. 2. The response was obtained from the ratio of $D_{SW}/\bar{D}_{nanoDot}$ and was normalized at the reference condition (depth: 10 cm, field size: 10 × 10 cm^2) for 6 MV photons. The nanoDot response increased as the photon energy decreased, and the field size increased. The response increased to 3% for a 20 × 20-cm^2 field at 4 MV, as shown in Fig. 2(a). This is attributed to an increase in the number of lower energy scattered photons for the larger fields. In contrast, the nanoDot response was lower for a small field of 5 × 5 cm^2. For the small field, the mean photon energy increased owing to the decrease in the scattered photons within the field. The response as a function of the depth was approximately constant, except for d_{max}. The field size and depth dependence of the nanoDot were determined by the mean photon energy in the phantom at the irradiation condition.

Fig. 3 presents the nanoDot response as a function of the mean photon energy which was calculated for each energy, field size, and depth. The nanoDot response was in a range from 1.0 to 0.99 for mean photon energy of more than 1.0 MeV but it increased with less than the 1.0 MeV

3.4. Burlin's general cavity theory for the nanoDot cavity material

The dose contribution from the photon interactions, (1-d), in the nanoDot cavity as a function of $TPR_{20,10}$ at a depth of 10 cm is shown in Fig. 4. The values of (1-d) decreased with an increasing photon energy and a decreasing field size. The values of (1-d) of the nanoDot were smaller than 0.526–0.174 (at the 10 × 10-cm^2 field for 4–18 MeV) in the radiophotoluminescent glass dosimeter (RGD) calculated by Araki et al. [28]. The sensitive material of Al_2O_3 in the nanoDot contained an effective atomic number of 11.28 and density of 1.41 g/cm^3. In contrast, those of the RGD were 12.04 and 2.64 g/cm^3, respectively. Therefore, the values of (1-d) in the nanoDot were smaller than those in the RGD.

The perturbation correction factor, P_Q, calculated from Eq. (4) at the depth and field size for 4–18 MV is shown in Fig. 5. The perturbation effects of the nanoDot disk (Al_2O_3) for the lower energy became larger with an increasing field size and depth owing to an increase in the scattered photons within the field. The parameter P_Q was approximately constant in a range of 0.96–0.97 for photon energies greater than 10 MV. However, P_Q decreased to 0.935–0.95 and 0.95–0.96 for the lower energies of 4 and 6 MV, respectively.

Fig. 6 presents P_Q as a function of mean photon energy. Values of P_Q were in a range of 0.96–0.97 for mean photon energy of more than 1.0 MeV. The energy dependence of P_Q corresponds to the nanoDot response in Fig. 3.

3.5. Angular dependence

The nanoDot response was normalized to that at 0°, which was a beam direction perpendicular to the nanoDot. The calculated angular dependences were in agreement within 2% with the measured values. The response at 90° and 270° decreased to approximately 5% and 3% for 6 MV and 15 MV, respectively. Kerns et al. [13] reported an angular dependence of approximately 4% and 3% for 6 MV and 18 MV, respectively. The variation of the response is attributed to the shape of the nanoDot disk. The primary photon fluence that interacts with the detector decreases when an incident beam is parallel to the disk. Kerns et al. [13] indicated that the dose deposited by low-energy electrons decreased to 1% when the detector was parallel to the beam (90° and 270°).

4. Conclusions

The energy response of the nanoDot for 4–18 MV photons was by 1.2% for 4-MV photons compared to 6-MV at the reference condition (depth: 10 cm, field size: 10 × 10 cm^2). The response increased by 3% based on the depth and field size. The response was almost independent of mean photon energy of more than 1.0 MeV. For the lower energy, the

perturbation effect became larger, and the dose contribution from the photon interactions increased. The perturbation factor was also almost independent of mean photon energy of more than 1.0 MeV. The nanoDot response was reduced by 5% and 3% at 6-MV and 15-MV photons for a parallel beam, respectively. The angular dependence correction factor should be decided based on irradiation angles.

Acknowledgments

The authors would like to thank Ph.D. Shimohigashi and the additional staff of the Department of Radiological Technology, Kumamoto University Hospital and R.T. Sakata and the additional staff of Kumamoto Radiosurgery Clinic for their assistance and helpful discussions related to this study.

References

[1] Dunn L, Lye J, Kenny J, et al. Commissioning of optically stimulated luminescence dosimeters for use in radiotherapy. Radiat Meas 2013;51–52:31–9.
[2] Lye J, Dunn L, Kenny J, et al. Remote auditing of radiotherapy facilities using optically stimulated luminescence dosimeters. Med Phys 2014;41.
[3] Alvarez P, Kry SF, Stingo F, et al. TLD and OSLD dosimetry systems for remote audits of radiotherapy external beam calibration. Radiat Meas 2017;106:412–5.
[4] Mrcela I, Bokulic T, Izewska J, et al. Optically stimulated luminescence in vivo dosimetry for radiotherapy: physical characterization and clinical measurements in 60Co beams. Phys Med Biol 2011;56:6065–82.
[5] Wesolowska PE, Cole A, Santos T, et al. Characterization of three solid state dosimetry systems for use in high energy photon dosimetry audits in radiotherapy. Radiat Meas 2017;106:556–62.
[6] Thistlethwaite J, Johnson D, Valentino DJ. microSTARiiTM – A new system for medical dosimetry; Part 1: Technology and Initial Performance. LANDAUER Technology Whitepaper; 2013.
[7] Yukihara E, Mardirossian G, Mirzasadeghi M, et al. Evaluation of Al2O3: C optically stimulated luminescence (OSL) dosimeters for passive dosimetry of high-energy photon and electron beams in radiotherapy. Med Phys 2008;35:260–9.
[8] Schembri V, Heijmen BJ. Optically stimulated luminescence (OSL) of carbon-doped aluminum oxide (Al_2O_3:C) for film dosimetry in radiotherapy. Med Phys 2007;34:2113–8.
[9] Viamonte A, da Rosa LA, Buckley LA, et al. Radiotherapy dosimetry using a commercial OSL system. Med Phys 2008;35(4):1261–6.
[10] Reft CS. The energy dependence and dose response of a commercial optically stimulated luminescent detector for kilovoltage photon, megavoltage photon, and electron, proton, and carbon beams. Med Phys 2009;36:1690–9.
[11] Scaboro SB, Followill DS, Kerns JR, et al. Energy response of optically stimulated luminescent dosimeters for non-reference measurement location in a 6 MV photon beam. Phys Med Biol 2012;57:2505–15.
[12] Kim DW, Chung WK, Shin DO, et al. Dose response of commercially available optically stimulated luminescent detector, Al2O3: C for megavoltage photons and electrons. Radiat Prot Dosim 2012;149:108–9.
[13] Kerns JR, Kry SF, Sahoo N, et al. Angular dependence of the nanoDot OSL dosimeter. Med Phys 2011;38:3955–62.
[14] Lehmann J, Dunn L, Lye JE, et al. Angular dependence of the response of the nanoDot OSLD system for measurements at depth in clinical megavoltage beams. Med Phys 2014;41:061712.
[15] Jursinic PA. Angular dependence of dose sensitivity of nanoDot optically stimulated luminescent dosimeters in different radiation geometries. Med Phys 2015;42:5633–41.
[16] Zakjevskii V, Knill C, Rakowski J, et al. Development and evaluation of an end-to-end test for head and neck IMRT with a novel multiple-dosimetric modality phantom. J Appl Clin Med Phys 2016;17:497–510.
[17] Loughery B, Knill C, Silverstein E, et al. Multi-institutional evaluation of end-to-end protocol for IMRT/VMAT treatment chains utilizing conventional linacs. Med Dosim 2018;18:30020–7.
[18] IAEA, Absorbed dose determination in external beam radiotherapy: An international code of practice for dosimetry based on standards for absorbed dose to water. Technical Report Series No. 398 (IAEA, Vienna, 2000).
[19] Wulff J, Zink K, Kawrakow I. Efficiency improvements for ion chamber calculations in high energy photon beams. Med Phys 2008;35:1328–36.
[20] Kawrakow I, Mainegra-Hing E, Tessier F, et al. EGSnrc c++ class library. National Research Council of Canada Report. 2018; No. PIRS-898.
[21] Rogers DW, Faddegon BA, Ding GX, et al. BEAM: a Monte Carlo code to simulate radiotherapy treatment units. Med Phys 1995;22:503–24.
[22] Rogers DW, Walters BR, Kawrakow I. BEAMnrc users Manual. National Research Council of Canada Report. 2018; No. PIRS-509 (A) revL.
[23] Burlin TE. A general theory of cavity ionization. Br J Radiol 1966;39:727–34.
[24] Spencer LV, Atixx FH. A theory of cavity ionization. Radiat Res 1955;3:239–54.
[25] Rogers DW, Kawrakow I, Mainegra-Hing E, et al. BRC User Code for EGSnrc. National Research Council of Canada Report. 2018; No. PIRS-702 (revC).
[26] Seltzer SM, Hubbell JH. Tables and graphs of photon mass attenuation coefficients and mass energy-absorption coefficients for photon energies 1 keV to 20 MeV for elements Z=1 to 92. NIST: The X-ray Attenuation and Absorption for Materials of Dosimetric Interest Database; 1995.
[27] Berger MJ, Hubbell JH. XCOM: Photon cross sections on a personal computer Report NBSIR87-3597. Gaithersburg, MD: National Institute of Standards Technology; 1987. p. 20899.
[28] Araki F, Ohno T. The response of a radiophotoluminescent glass dosimeter in megavoltage photon and electron beams. Med Phys 2014;41:122102.